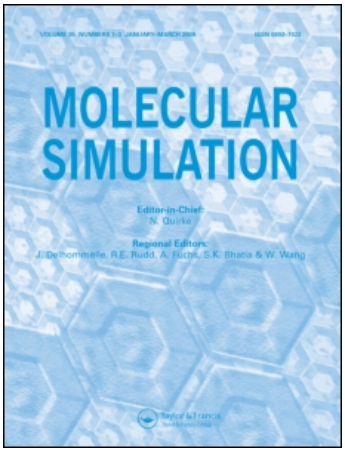

Molecular Simulation
Publication details, including instructions for authors and subscription information:
http://www.informaworld.com/smpp/title~content=t713644482

Influence of Gas-Solid Kinetic Energy Exchange Processes on Gas Effusion from Slitpores in Non-equilibrium Molecular Dynamics Simulations

Shin-ichi Furukawa[a]; Akira Fukui[a]; Yi Zhang[a]; Tomoshige Nitta[a]
[a] Department of Materials Engineering Science, Graduate School of Engineering Science, Osaka University, Osaka, Japan

To cite this Article Furukawa, Shin-ichi , Fukui, Akira , Zhang, Yi and Nitta, Tomoshige(2004) 'Influence of Gas-Solid Kinetic Energy Exchange Processes on Gas Effusion from Slitpores in Non-equilibrium Molecular Dynamics Simulations', Molecular Simulation, 30: 6, 379 — 385
To link to this Article: DOI: 10.1080/08927020310001659935
URL: http://dx.doi.org/10.1080/08927020310001659935

Molecular Simulation, Vol. 30 (6), 15 May 2004, pp. 379–385

Taylor & Francis
Taylor & Francis Group

Influence of Gas–Solid Kinetic Energy Exchange Processes on Gas Effusion from Slitpores in Non-equilibrium Molecular Dynamics Simulations

SHIN-ICHI FURUKAWA, AKIRA FUKUI, YI ZHANG and TOMOSHIGE NITTA*

Department of Materials Engineering Science, Graduate School of Engineering Science, Osaka University, Toyonaka, Osaka 560-8531, Japan

(Received May 2003; In final form November 2003)

The boundary-driven type non-equilibrium molecular dynamics (BD-NEMD) simulations have been carried out to clarify the influence of solid flexibility on gas effusion through a slitpore, by using a rigid solid model (R-model) and a flexible solid model (F-model). The LJ potential particles with parameters of argon are chosen for both the effusing gas molecules and the solid atoms. It is found that the R-model combined with a velocity scaling technique provides a reasonable effusion flux, probably a maximum in magnitude, compared with the fluxes calculated from the F-model without a fictitious thermostat (a velocity scaling) for effusing molecules. In the F-model, temperature lowering has been observed at the pore exit, being enhanced with an increase in the strength of springs that unite the solid atoms. This observation indicates that the molecules escaping from the pore exit take the excess kinetic energy for evaporation from solid atoms or surrounding molecules, which results in the low exit temperature, and that the rate of gas–solid kinetic energy exchange decreases with increasing spring strength (i.e. decreasing solid flexibility). It is suggested that the effusion flux is influenced by two factors: the solid flexibility and the molar potential energy in the pore.

Keywords: Non-equilibrium molecular dynamics; Energy exchange; Effusion; Membrane

INTRODUCTION

Membrane separations have been intensively investigated because of their several advantages over other separation processes: low energy consumption and the compactness of separation plants [1,2]. Understanding permeation and separation mechanisms from the viewpoints of the diffusion and the adsorption is important for rational design of membranes. Recently, several molecular simulation techniques consisting of molecular dynamics (MD) and Monte Carlo (MC) methods [3,4] have been utilized for studies of permeation mechanisms at the molecular level; in particular, a boundary-driven type non-equilibrium molecular dynamics (BD-NEMD) technique [5–10] has been widely used [10–19] since it is simple and easy to generate non-equilibrium stationary states by deposing two control regions in a simulation cell.

In most BD-NEMD simulations for gas permeation, membrane atoms have been fixed at their stable locations, providing potential fields for permeating molecules without exchange of kinetic energies. Therefore, these NEMD simulations have to employ some temperature correction techniques, such as the velocity scaling or the Nose-Hoover thermostat techniques [3,4], to take into consideration the kinetic energy exchange between solid atoms and diffusing molecules. However, there have been no reports that examine the reliability of these corrections in NEMD simulations of molecular transport through micro-pores.

As for the equilibrium-MD simulations, Demontis *et al.* [20–22] have investigated effects of framework vibrations on diffusion of methane in zeolite crystallites, by comparing with rigid and flexible framework models. According to their simulation results, the values of diffusivity of methane obtained from the flexible framework model were almost the same as those from the rigid framework model, though some differences were observed in the shape

*Corresponding author. Tel./Fax: +81-6-6850-6265. E-mail: nitta@cheng.es.osaka-u.ac.jp

ISSN 0892-7022 print/ISSN 1029-0435 online © 2004 Taylor & Francis Ltd
DOI: 10.1080/08927020310001659935

of the mean-square-displacement (MSD) curves. They also suggested that the similarity of methane diffusivities might be ascribed to the small size of diffusing molecules compared with the windows of zeolites and that the small differences in the MSD curve shape might be due to the movable potential energy barriers through the adjustment of framework atoms to diffusing molecules. However, there have been no reports that deal with the effect of the strength of springs that connect framework atoms, which will influence the effusion rate, in particular, by changing the rate of kinetic energy exchange between solid atoms and molecules as well as the potential barriers for diffusion.

In this work, we carry out BD-NEMD simulations to investigate the influence of the flexibility of solid atoms on gas effusion through a slitpore, by using a rigid solid model (R-model) combined with the velocity scaling technique and a flexible solid model (F-model) without a fictitious thermostat for effusing molecules. For the R-model, the MD step interval for the velocity scaling is chosen as a simulation parameter from the viewpoint of practical importance of simulations while the flexibility of membrane atoms is chosen for the F-model from physical significance on the effusion process.

SIMULATION DETAILS

Figure 1 shows a schematic diagram of the simulation cell used in this work for investigation of gas effusion through a slit-shaped pore. The pore is dug in the center of face-centered cubic (f.c.c.) crystal of argon atoms. The shape of the cross section of the pore (or channel) is slightly zigzag at the atomic scale. The simulation cell consists of two areas: the condensed area of membrane atoms with a pore and two space areas representing the gas phase connected to the molecular sinks (L-regions). In order to apply the periodic boundary conditions in three dimensions, the condensed area is divided into two parts, each with an equal number of membrane atoms. Furthermore, two H-regions are set to be adjacent in the center of the cell as shown in the figure. Two L-regions are sinks of diffusing molecules, that is, molecules that enter into the L-regions are immediately removed from the cell. On the other hand, the H-regions are molecular sources where the chemical potentials of the diffusing component are kept constant by using insertion/deletion algorithms of the μVT-ensemble Monte Carlo (μVT-MC) technique. In the M-regions, which locate between the H-region and the L-region, molecules can diffuse through the membrane into evacuated space without any manipulation of local molecular densities. It is noted here that, in our previous paper [19], we used the μVT-MC technique to maintain the number of molecules in the H-region to reduce the computation cost; however, in this work, we have adopted the algorithm that keeps the chemical potential of the H-region as proposed by Heffelfinger *et al.* [6] for making rational comparisons of simulation results calculated for both rigid and flexible membranes consisting of different strength of springs that unite membrane atoms.

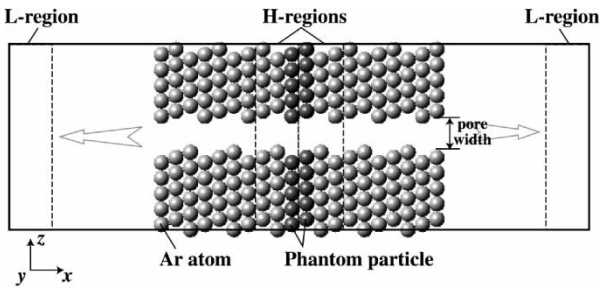

FIGURE 1 Schematic diagram of the simulation cell for gas effusion through a slitpore.

One μVT-MC cycle consists of 100 insertion/deletion trials and it is carried out at every 50 MD steps. The velocities of inserted molecules are assigned with random numbers on the Gaussian distribution. In addition, a so-called streaming velocity (v_{st}) [10,13,15] is added to the inserted molecules to eliminate the discontinuity in the flux at the interface between the H-region and the M-region. At the end of each μVT-MC cycle, the velocities of all molecules in the H-region are rescaled in three directions independently so as to maintain a constant temperature of molecules in the H-region. For the operation of velocity scaling, the streaming velocity in the x-direction is eliminated first and added after the scaling.

The streaming velocity v_{st} is recalculated at every MD block, which consists of 1000 MD steps, as the block-average flux in the M-region divided by the block-average density in the H-region, both are on the basis of the last MD block

$$v_{st} = \frac{\langle J^M \rangle_{\text{MD block}}}{\rho^{CR}}, \quad J^M = \rho^M \times \frac{\sum_{i \in \text{M-region}} v_i}{N^M} \qquad (1)$$

where J^M, N^M and ρ^M are the molar flux, the number of molecules, and the density, respectively, in the M-region, ρ^{CR} is the density of the control region (the H-region in this case), and v_i is the velocity of ith molecule.

The solid membrane is modeled by first arranging argon atoms in the f.c.c. crystal structure and then removing the atoms in the direction perpendicular to the (111) surface. The slit width of the pore is set at 0.66 nm. Two types of solid models are adopted: a Rigid model (R-model) and a Flexible model (F-model). In the R-model, the solid atoms are fixed

at their optimized locations. Therefore, in order to take account of the kinetic energy exchanges between the solid and the gas, the velocities of all the molecules moving in each subcell are simultaneously rescaled so as to keep a constant temperature of the molecules in each subcell. We divided the M-region into 10 subcells in the x-direction. It should be noted that this velocity scaling procedure may correspond to infinitely rapid exchange of kinetic energies between the molecules and the solid atoms.

In the F-model, the solid atoms are movable through springs of harmonic oscillators; the potential function for a pair of adjacent atoms, E_p^s, is given as [23],

$$E_p^s = \frac{1}{2}k_s(r - r_0)^2 \tag{2}$$

where k_s is the spring constant, r the distance between solid atoms, and r_0 the equilibrium inter-atomic distance ($= 0.381$ nm). The value for k_s is 8.89 N/m taken from the constant of platinum [24]. In the F-model, the kinetic energies are exchanged between the solid atoms and effusing molecules through both collisions and interactions between atoms and molecules while the energy transfer in the solid entity is also conducted through direct collisions of solid atoms. As shown in Fig. 1, a part of solid atoms in the H-regions are replaced by phantom particles [25,26], with a dumping constant ($= 4.23 \times 10^{-13}$ kg/s) [23] so as to introduce a thermostat for the solid atoms.

The effusing molecules and the solid atoms are represented as the Lennard–Jones particles with potential parameters of argon ($\sigma = 0.3405$ nm, $\varepsilon = 1.006$ kJ/mol) [23]. The cut-off distance for calculations of the intermolecular interactions is set at 1.0 nm. The size of a simulation cell is $12.4 \times 9.91 \times 3.96$ nm^3 and the thickness of the control regions is 1.0 nm. The chemical potential of an effusing gas in the H-region ($P_H = 10$ MPa) is calculated through the ideal gas law. All the NEMD simulations are conducted by integrating the classical equations of motion using the Verlet technique of the velocity form with 1.0 fs for the time increment of an MD step. To calculate the ensemble averages of density, potential energy, and effusion flux in a stationary state, the last 500,000 MD steps in total 1,000,000 MD steps have been adopted.

RESULTS AND DISCUSSION

In the simulations for the R-model, the interval of MD steps for one velocity rescaling operation (Rescaling MD Interval: RI) is varied at three levels (RI = 1, 10 and 100 steps). For the F-model, the strength of the springs is varied at three levels by multiplying the strength factor α (= 0.1, 1.0, 10.0) to the original spring constant k_s (= 8.89 N/m). It is noted that the MD step time of 1.0 fs is confirmed to be small enough for simulating vibrations of solid atoms even in the case of the largest spring constant ($\alpha = 10.0$) by the conduction of BD-NEMD simulations with smaller MD step times (0.25 and 0.5 fs). In all the simulations, the temperature is set at 298 K.

Figure 2 shows snapshots and molecular trajectories for the R-model (RI = 1 step) and the F-model ($\alpha = 0.1$). The trajectories are drawn for all molecules in the right hand side of the simulation cell during a time interval of 20 ps. In the two solid models, the molecules effusing from the pore exit are either trapped on the outer surface of the solid or dispersed directly into the gas phase. In the F-model, the solid atoms vibrate around their

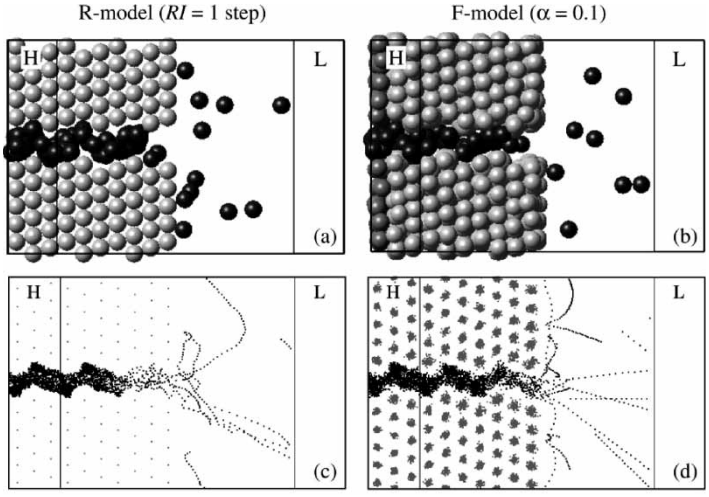

FIGURE 2 Snapshots (a, b) and molecular trajectories (c, d) for the R-model (RI = 1 step) and the F-model ($\alpha = 0.1$); $\Delta t = 20$ ps for molecular trajectories.

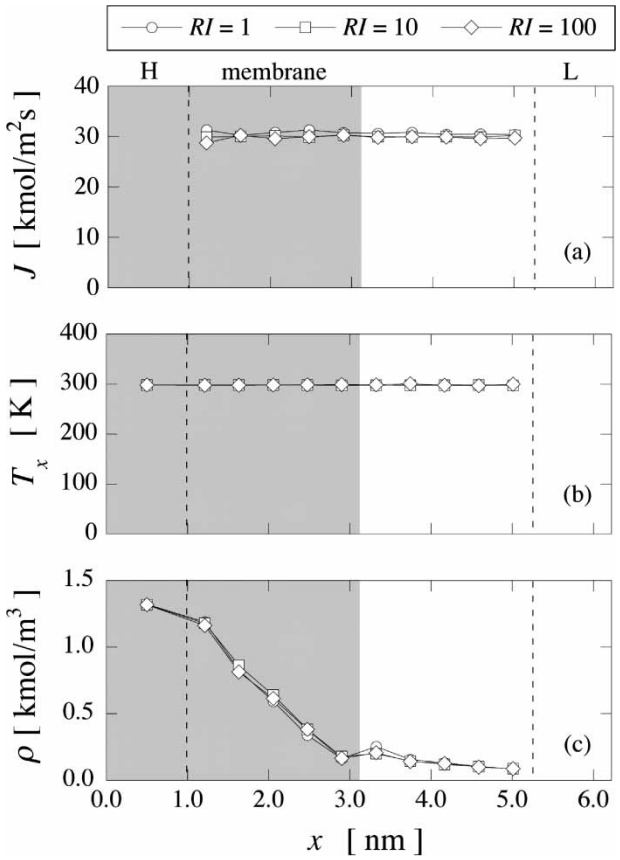

FIGURE 3 Profiles of effusion flux (a), internal temperature in the x-direction (b) and local density (c) for the R-model.

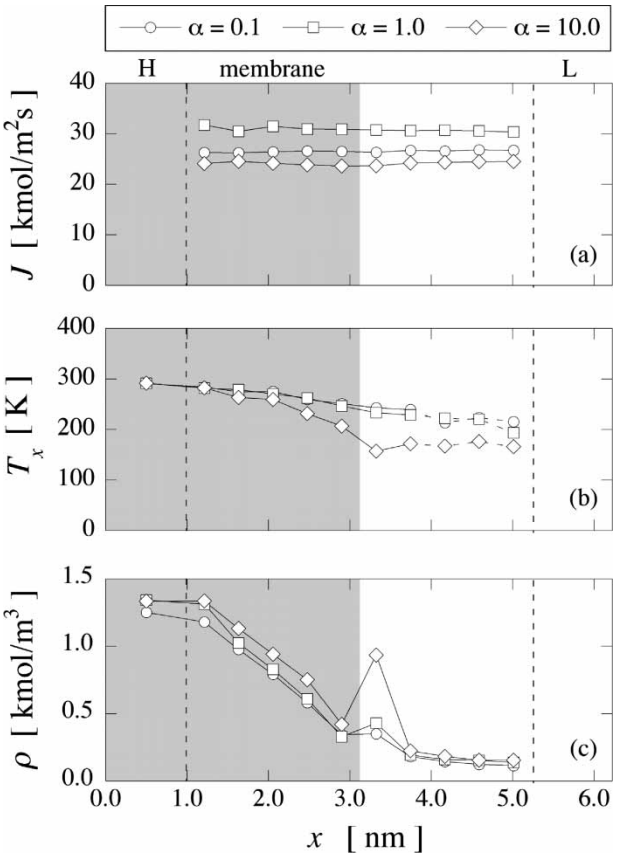

FIGURE 4 Profiles of effusion flux (a), internal temperature in the x-direction (b) and local density (c) for the F-model.

equilibrium positions. It is observed that the vibration amplitudes of surface atoms, locating at either the inner surface of the pore or the outer surface of the solid, are larger than those of inside atoms, which is ascribed to the small number of springs connecting to a surface atom.

Figure 3a–c shows the profiles of the effusion flux (J), the internal temperature in the x-direction (T_x), and the local density (ρ), respectively, for the R-model. The internal temperature of each subcell (T_x^{SC}) is calculated from the molecular velocities (v_i) subtracted by the local stream velocity in the subcell ($v_{\mathrm{st}}^{\mathrm{SC}}$), which are defined as follows:

$$T_x^{\mathrm{SC}} = \frac{\sum_{i\in\mathrm{SC}} m_i\left(v_i - v_{\mathrm{st}}^{\mathrm{SC}}\right)^2}{N^{\mathrm{SC}}k_{\mathrm{B}}}, \quad v_{\mathrm{st}}^{\mathrm{SC}} = \frac{\sum_{i\in\mathrm{SC}} v_i}{N^{\mathrm{SC}}} \qquad (3)$$

where m_i, is the mass of molecule i, N^{SC}, the number of molecules in the subcell, k_{B}, Boltzmann constant. The subcell width in the x-direction is 4.22 nm. As shown in Fig. 3a,b, the profiles of J and T_x are almost constant in the whole simulation cell and they coincide with each other regardless of the rescaling MD interval (RI), which indicates that the velocity scaling technique has worked well in each simulation run and that the rescaling interval in MD Steps can be taken as long as 100 steps to obtain a reliable value for the effusion flux in the R-model. In Fig. 3c, three curves of ρ behave similarly; that is, they sharply decrease in the pore towards the membrane exit, then slightly increase at the outer surface due to adsorption on it, and finally they decrease towards the sink. The sharp and large decrease in the density in the pore indicates that the diffusion process of molecules passing through the zigzag pore is the largest resistance for effusion to gas phase compared with other processes: direct evaporation at the exit or desorption from the outer solid surface.

Figure 4a–c shows the profiles of J, T_x and ρ, respectively, for the F-model with different values of 0.1, 1.0 and 10.0 for the spring strength factor α. At the first glance, three curves for effusion flux J are constant in the whole simulation cell though they are different in magnitude. A largest value of 31 kmol/m^{2}s for J is obtained for $\alpha = 1.0$, which is the same flux obtained for the R-model. This is good information for BD-NEMD simulation since the R-model is less costly than the F-model.

In Fig. 4b, the curves for T_x, calculated from Eq. (3), decrease towards the effusion direction, especially in the pore region; the decreases are small and almost identical for $\alpha = 0.1$ and 1.0 while it is much larger for $\alpha = 10.0$ than the other two. This temperature lowering was unexpected; however,

it is interpreted in terms of heat of evaporation (or desorption) and the heat transfer rate that govern the effusion process at the pore exit; that is, a molecule effusing from the pore exit to the gas phase has to take extra kinetic energy necessary to evaporate (or desorb) from either solid atoms or surrounding molecules; therefore, the temperature of molecules remaining at the exit gets lowered unless the heat (kinetic energy) is fully supplied from the solid. Therefore, large temperature lowering observed for a flexible solid with strong springs ($\alpha = 10.0$) indicates that the rate of gas–solid kinetic energy exchange decreases with increasing spring strength (i.e. decreasing solid flexibility). Another description is possible for the effusion process in the case of rather rigid solid; that is, collisions of molecules on to solid atoms are likely elastic and little heat flows from solid to molecules, resulting in temperature lowering of molecules that have given their kinetic energies to the effused molecules. It is noted here that, in Fig. 4b, the four points in the gas region are connected by broken lines since the velocity distributions in these regions are significantly deviated from the Gaussian function, which will be shown later.

In Fig. 4c, density profiles for the three spring models are almost the same except in the case of $\alpha = 10.0$, where the local density at the outer surface is much higher than others, which is consistent with the finding of large temperature lowering at the outer surface; that is, as the temperature lowers at the outer surface, molecules lose their frequency to get excess kinetic energy for desorption and the density increases. Another explanation from the statistical viewpoint could be plausible; that is, the Boltzmann factor increases with lowering temperature, which results in the increase in the adsorption density at the outer surface.

Figure 5 shows the molecular velocity distributions for the F-model with $\alpha = 10$ in the H-region (denoted as H) and four subcells in the M-region (denoted as 2, 4, 6 and 8), the locations of each subcell are displayed at the top of the figure. Each arrow in the figure denotes the center of velocity distribution, which corresponds to the stream velocity in each subcell. The velocity distribution in the H-region is perfectly Gaussian and the center velocity slightly shifts to the positive direction, which is the streaming velocity automatically given in the NEMD simulation. As molecules go downward, the pore passing through subcells 2 and 4, the center velocity increases due to the decrease in the local density while the distribution curve keeps the Gaussian shape. Almost the same curve is obtained in subcell 6, which includes the outer surface of the solid. The distribution curve in subcell 8, on the other hand, shows significant asymmetry as the backward velocities are almost cut, indicating that molecules

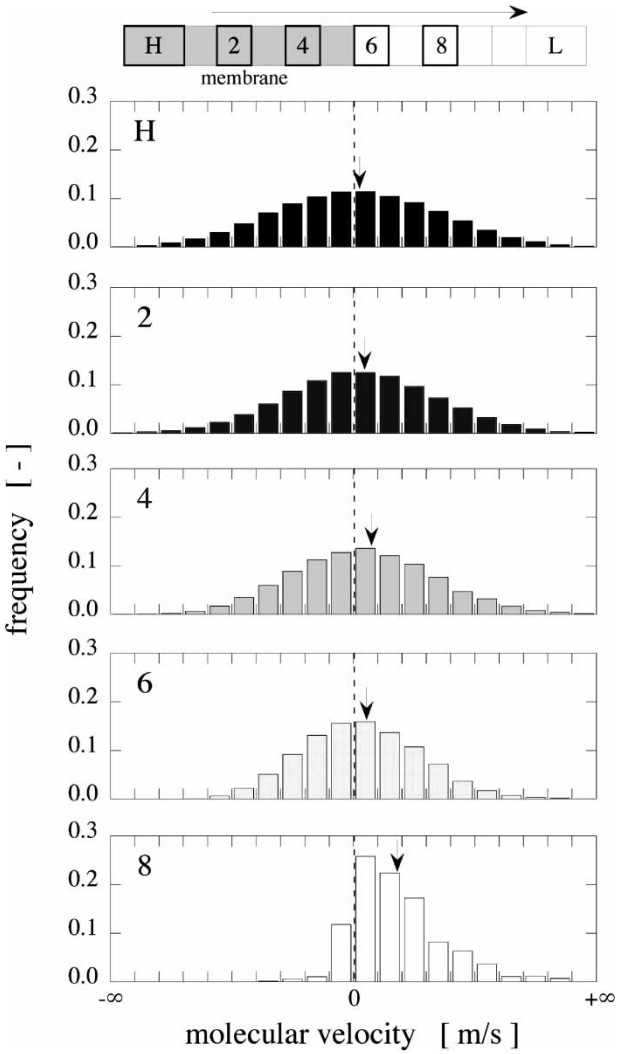

FIGURE 5 Molecular velocity distributions in the H-region and four subcells numbered as 2, 4, 6 and 8 in the M-region for the F-model ($\alpha = 10$); an arrow in each figure indicates the center of distribution.

moving into this region infrequently go back due to small attractive force exerted from the solid surface. Therefore, we conclude that the internal temperatures T_x calculated through Eq. (3) are reliable only for subcells 1–6, slightly doubtful for subcell 7, and unreliable for subcells 8–10; This is the reason why we used broken lines in Fig. 4 for connecting the data points at subcells 8–10; furthermore, the Gaussian distribution curve for subcell 6 is good evidence for the local equilibrium in the small region at the outer surface.

To have more insight into the potential energy of molecules, we calculated the local molar potential energies (E_p) issued from interactions between molecule–molecule (gas–gas) and molecule–solid atoms (gas–solid); they are shown in Fig. 6 for the F-model with three values for α. The three curves for E_p (gas–gas) are almost identical, increasing from the inside of the pore to the gas phase due to

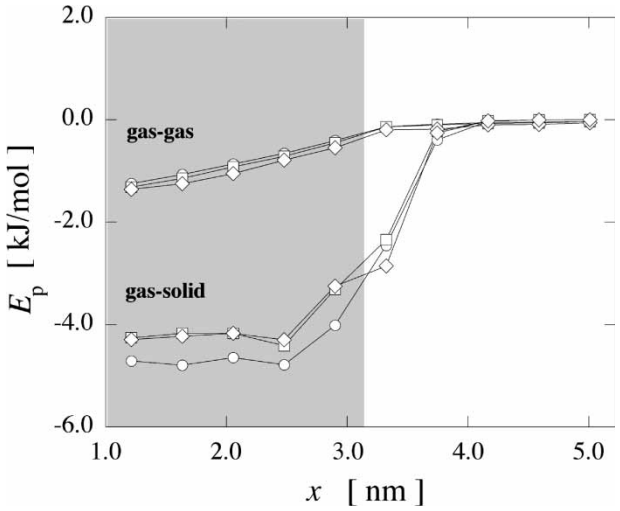

FIGURE 6 Profiles of molar potential energies due to interactions between diffusing molecules (gas–gas) and molecule–solid atoms (gas–solid) in the M-region for the F-model.

the decrease in the local density. As for the E_p (gas–solid), two curves for $\alpha = 1.0$ and 10.0 are almost the same inside the pore region while the curve for $\alpha = 0.1$, corresponding to weak springs, is lower than others, which indicates that the more flexible the membrane atoms, the deeper the E_p (gas–solid) since atoms can adjustably move so as to obtain the lower potential energy.

Figure 7 shows the effect of the spring strength factor α on the average effusion flux J for the F-model. Though the data points are only three, they are reliable to reach the conclusion that there exists a maximum in J in the vicinity of $\alpha = 1.0$. It is noted that the original value for k_s taken from the spring constant of platinum crystal [24] might have been so lucky for us to obtain the significant result. Now, we have macroscopic and molecular level knowledge from simulations to understand the reason why the maximum exists in J with the change of spring strength for the F-model. When the spring is very strong as in the case of $\alpha = 10.0$, the kinetic energies are exchanged weakly between molecules and solid atoms, which results in both temperature lowering at the membrane exit and the decrease in frequency for molecules to evaporate or desorb into gas phase. On the other hand, when the spring is weak as in the case of $\alpha = 0.1$, the exchange rate of kinetic energies becomes high and temperature lowering becomes low; however, the potential energy of molecules in the pore becomes deeper due to the high flexibility of solid atoms, which increases the potential barrier for molecules to evaporate or desorb from the membrane exit since they have to gather more excess kinetic energy to escape to the vacuum.

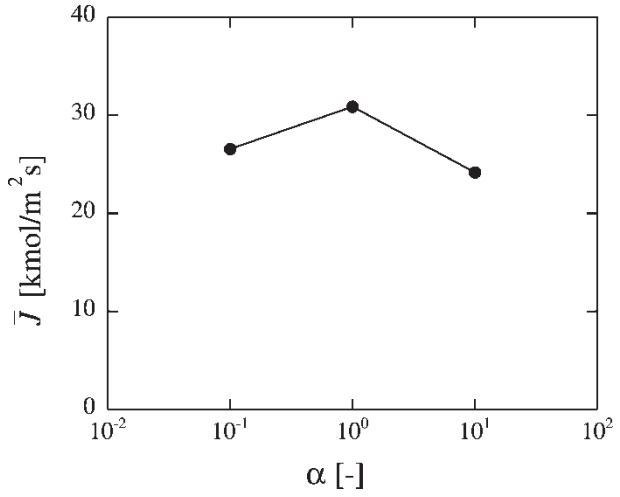

FIGURE 7 Average effusion flux against the spring strength factor of solid atoms for the F-model.

CONCLUSIONS

We have carried out BD-NEMD simulations of gas effusion through a slitpore by using two types of solid models: the R-model combined with a velocity scaling technique and the F-model without a fictitious thermostat for effusing molecules. The LJ potential particles with parameters of argon were chosen for both effusing gas and solid atoms. In the BD-NEMD simulations, the chemical potentials at two control H-regions were kept at a specified value and the streaming velocity was added on the inserted molecules.

It is concluded that the R-model combined with a velocity scaling technique provides a reasonable effusion flux, probably a maximum in magnitude, compared with the fluxes obtained from the F-model with different strengths of springs that unite solid atoms. In the F-model, temperature lowering was observed at the pore exit where effusing molecules must take excess kinetic energy from solid atoms or surrounding molecules to evaporate into the gas phase. Temperature lowering is enhanced with an increase in the strength of the spring, which indicates that substantially rigid solid with strong springs hardly exchange the kinetic energy between solid and gas. On the other hand, a weak spring provides another effect on the potential energy; that is, when solid atoms are too flexible, the molar potential energy becomes low in magnitude, which results in the decrease in effusion flux due to the increase in the potential barrier for molecules to escape from the pore exit.

References

[1] Caro, J., Noack, M., Kolsch, P. and Schafer, R. (2000) "Zeolite membranes—state of their development and perspective", *Microp. Mesop. Mat.* **38**, 3–24.

[2] Ismail, A.F. and David, L.I.B. (2001) "A review on the latest development of carbon membranes for gas separation", *J. Mem. Sci.* **193**, 1–18.
[3] Allen, M.P. and Tildesley, D.J. (1987) *Computer Simulation of Liquids* (Clarendon Press, UK).
[4] Frenkel, D. and Smit, B. (1996) *Understanding Molecular Simulation: From Algorithm to Applications* (Academic Press, USA), revised ed. 2001.
[5] Hafskjold, B., Ikeshoji, T. and Ratkje, S.K. (1993) "On the molecular mechanism of thermal-diffusion in liquids", *Mol. Phys.* **80**, 1389–1412.
[6] Heffelfinger, G.S. and van Swol, F. (1994) "Diffusion in Lennard–Jones fluids using dual control-volume grand-canonical molecular-dynamics simulation (DCV-GCMD)", *J. Chem. Phys.* **100**, 7548–7552.
[7] MacElroy, J.M.D. (1994) "Nonequilibrium molecular dynamics simulation of diffusion and flow in thin microporous membranes", *J. Chem. Phys.* **101**, 5274–5280.
[8] Cracknell, R.F., Nicholson, D. and Quirke, N. (1995) "Direct molecular-dynamics simulation of flow down a chemical-potential gradient in a slit-shaped micropore", *Phys. Rev. Lett.* **74**, 2463–2466.
[9] Furukawa, S., Shigeta, T. and Nitta, T. (1996) "Non-equilibrium molecular dynamics for simulating permeation of gas mixtures through nanoporous carbon membranes", *J. Chem. Eng. Jpn.* **29**, 725–728.
[10] Arya, G., Chang, H.C. and Maginn, E.J. (2001) "A critical comparison of equilibrium, non-equilibrium and boundary-driven molecular dynamics techniques for studying transport in microporous materials", *J. Chem. Phys.* **115**, 8112–8124.
[11] MacElroy, J.M.D. and Boyle, M.J. (1999) "Non-equilibrium molecular dynamics simulation of carbon membrane separation of CH_4/H_2 mixtures", *Chem. Eng. J.* **74**, 85–97.
[12] Pohl, P.I. and Heffelfinger, G.S. (1999) "Massively parallel molecular dynamics simulation of gas permeation across porous silica membranes", *J. Mem. Sci.* **155**, 1–7.
[13] Xu, L., Sedigh, M.G., Tsotsis, T.T. and Sahimi, M. (2000) "Non-equilibrium molecular dynamics simulation of transport and separation of gases in carbon nanopores. II. Binary and ternary mixtures and comparison with experimental results", *J. Chem. Phys.* **112**, 910–922.
[14] Chandross, M., Webb, E.B., Grest, G.S., Martin, M.G., Thompson, A.P. and Roth, M.W. (2001) "Dynamics of exchange at gas–zeolite interfaces I: pure component *n*-butane and isobutane", *J. Phys. Chem. B* **105**, 5700–5712.
[15] Martin, M.G., Thompson, A.P. and Nenoff, T.M. (2001) "Effect of pressure, membrane thickness, and placement of control volumes on the flux of methane through thin silicalite membranes: a dual control volume grand canonical molecular dynamics study", *J. Chem. Phys.* **114**, 7174–7181.
[16] Yoshioka, T., Tsuru, T. and Asaeda, M. (2001) "Molecular dynamics studies on gas permeation properties through microporous silica membranes", *Sep. Pur. Tech.* **25**, 441–449.
[17] Takaba, H., Matsuda, E., Nair, B.N. and Nakao, S. (2002) "Molecular modeling of gas permeation through an amorphous microporous silica membrane", *J. Chem. Eng. Jpn.* **35**, 1312–1321.
[18] Zhang, Q., Zheng, J., Shevade, A., Zhang, L., Gehrke, S.H., Heffelfinger, G.S. and Jiang, S. (2002) "Transport diffusion of liquid water and methanol through membranes", *J. Chem. Phys.* **117**, 808–818.
[19] Furukawa, S. and Nitta, T. (2003) "A study of permeation of *n*-butane in ZSM-5 by using Monte Carlo and equilibrium/non-equilibrium molecular dynamics simulations", *J. Chem. Eng. Jpn.* **36**, 313–321.
[20] Demontis, P., Suffritti, G.B. and Mura, P. (1992) "A molecular dynamics study of diffusion of methane in silicalite molecular sieve at high dilution", *Chem. Phys. Lett.* **191**, 553–560.
[21] Demontis, P. and Suffritti, G.B. (1994) "Molecular dynamics investigation of the diffusion of methane in a cubic symmetry zeolite of type ZK4", *Chem. Phys. Lett.* **223**, 355–362.
[22] Fritzshe, S., Wolfsberg, M., Haberlandt, R., Demontis, P., Suffritti, G.B. and Tilocca, A. (1998) "About the influence of lattice vibrations on the diffusion of methane in a cation-free LTA zeolite", *Chem. Phys. Lett.* **296**, 253–258.
[23] Ohara, T. and Suzuki, D. (2000) "Intermolecular energy transfer at a solid–liquid interface", *Microscale Thermophys. Eng.* **4**, 189–196.
[24] Maruyama, S. and Kimura, T. (1999) "A study on thermal resistance over a solid–liquid interface by the molecular dynamics method", *Thermal Sci. Eng.* **7**, 63–68.
[25] Tully, J.C. (1980) "Dynamics of gas–surface interactions: 3D generalized Langevin model applied to fcc and bcc surfaces", *J. Chem. Phys.* **73**, 1975–1985.
[26] Blomer, J. and Beylich, A.E. (1996) "MD-Simulation of inelastic molecular collision with condensed matter surfaces", *Proc. Int. Symp. Rarefied Gas Dyn.*, 392–397.